

# A simple model of river meandering and its comparison to natural channels

Stephen T. Lancaster<sup>1\*</sup> and Rafael L. Bras<sup>2</sup>

<sup>1</sup>Department of Geosciences, Oregon State University, Corvallis, OR, 97331, USA

<sup>2</sup>Department of Civil and Environmental Engineering, Massachusetts Institute of Technology, Cambridge, MA 02139, USA

---

## Abstract:

We develop a new method for analysis of meandering channels based on planform sinuosity. This analysis objectively identifies three channel reach lengths based on sinuosity measured at those lengths: the length of typical, simple bends; the length of long, often compound bends; and the length of several bends in sequence that often evolve from compound bends to form multi-bend loops. These lengths, when normalized by channel width, tend to fall into distinct and clustered ranges for different natural channels. Mean sinuosity at these lengths also falls into distinct ranges. That range is largest for the third and greatest length, indicating that, for some streams, multi-bend loops are important for planform sinuosity while, for other streams, multi-bend loops are less important. The role of multi-bend loops is seldom addressed in the literature, and they are not well predicted by previous modeling efforts. Also neglected by previous modeling efforts is bank-flow interaction and its role in meander evolution. We introduce a simple river meandering model based on topographic steering that has more in common with cellular approaches to channel braiding and landscape evolution modeling than to rigorous, physics-based analyses of river meandering. The model is sufficient to produce reasonable meandering channel evolution and predicts compound bend and multi-bend loop formation similar to that observed in nature in both mechanism and importance for planform sinuosity. In the model, the tendency to form compound bends is sensitive to the relative magnitudes of two lengths governing meander evolution: (i) the distance between the bend cross-over and the zone of maximum bank shear stress, and (ii) the bank shear stress dissipation length related to bank roughness. In our simple model, the two lengths are independent. This sensitivity implies that the tendency for natural channels to form compound bends may be greater when the banks are smoother. Copyright © 2002 John Wiley & Sons, Ltd.

KEY WORDS fluvial geomorphology; river meandering

## INTRODUCTION

River meandering is a complicated process involving the interaction of flow through channel bends, bank erosion, and sediment transport. Some aspects of this process are better understood than others. Studies at the spatial scale of one to several bends (bend scale) and times that are short relative to the time from bend inception to cut-off (bend lifetime) are relatively numerous and have led to a detailed understanding of flow through channel bends and the interaction between that flow and the bed (e.g., Johannesson and Parker, 1989a,b,c; Smith and McLean, 1984; Nelson and Smith, 1989a,b; Blondeaux and Seminara, 1985; Seminara and Tubino, 1989, 1992; Imran *et al.*, 1999). The previous studies did not address the interaction between the flow and the bank, the interaction that produces bank shear stress and bank erosion. Thorne and Osman (1988) did study the effect of bank stability on bed form and, thus, one effect of the bank on the flow, but Thorne and Furbish (1995) showed that bank roughness affects the flow field and its interaction with the bank. Nelson and Smith (1989b) noted that consideration of lateral boundary effects would be necessary to extend their model to simulation of meandering.

---

\*Correspondence to: S.T. Lancaster, Department of Geosciences, Oregon State University, 3200 SW Jefferson Way, Corvallis, OR, 97331, USA. E-mail: Stephen.Lancaster@orst.edu

Another relatively poorly understood aspect of meandering is channel planform complexity. Meandering produces channel planforms that are relatively simple and recognizable at the bend scale but relatively complex and baffling at the scale of many, e.g., 100, bends (reach scale). A major contributor to planform complexity is compound bend formation, i.e., the “cumuliform” shapes noted by Howard (1992), the “compound bends” observed by Brice (1974), and the “lobing” and “double heading” studied by Hooke and Harvey (1983) among others. We define compound bends as bends that evolve from simple bends to develop a curvature reversal in the course of the bend (Figure 1). Brice (1974) showed with successive aerial photographs of the White River, IN, that a compound bend evolved from a simple bend following rapid downstream migration of the upstream bend. Our own analysis of aerial photography of the Ellis River, ME, shows this mechanism for two compound bends (Figure 1). Compound bends often lead to bend separation and the formation of larger cumuliform shapes, i.e., multi-bend loops (Figure 1), and Hooke and Harvey (1983) stated, “[Compound bend formation] is the major process whereby new bends develop.”

A new measure of channel planforms, developed herein, shows that the phenomenon of compound bend and multi-bend loop formation (i) occurs at characteristic channel length-scales, (ii) adds secondary and tertiary sinuosity to the planform, and (iii) varies in its importance among different streams.

Previous studies have reached different conclusions regarding the mechanism for compound bend formation. Hooke and Harvey (1983) and Thompson (1986) both asserted that a single pool-riffle unit cannot be

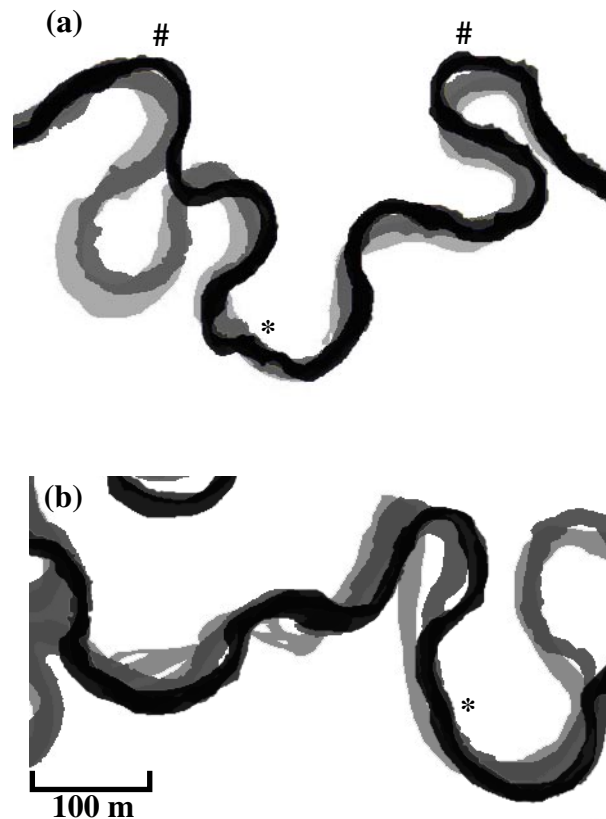


Figure 1. Examples of channel planforms and evolution at two locations, (a) and (b), on the Ellis River in Maine. Channels were extracted from aerial photographs and superimposed; light gray is 1943, dark gray is 1965, and black is 1992; flow is from left to right. In (a) a series of simple bends and one compound bend (\*) form a multi-bend loop (between # symbols). In (a) and (b) the time sequence shows compound bend formation. In both cases, cut-off of an upstream bend and a subsequent ‘wave’ of rapid downstream migration lead to curvature reversal at (\*), where curvature was low before the cut-off occurred. Field reconnaissance at site (a) confirmed that the bank material is homogeneous

sustained in longer bends but disagreed on the mechanism for subdivision of pools by new riffles, the former attributing it to the non-sustainability of the necessary secondary flows and the latter to the kinematics of sediment transport. Both studies concluded that the formation of new pool-riffle sequences preceded, and caused, compound bend formation. Ferguson (1984) found that compound bends could be the result of decreasing migration rate with curvature greater than some threshold, as observed by Nanson and Hickin (1983), but the physical mechanism for this decrease is uncertain. Furthermore, Furbish (1988) shows that the same data confirm that migration rate increases monotonically with curvature when bend length is accounted for, and Furbish (1991) concludes that there is no preferred, shorter bend length except in rare cases when the transverse bed slope is unusually small. This result would imply, however, that compound bend formation is rare, contrary to the observations of many authors including those cited above.

Previous physically based models, in their simplest forms, do not reproduce compound bends or cumuliform shapes. Sun *et al.* (1996) invoked heterogeneity of bank erodibility to explain cumuliform shapes. They ran the Johannesson and Parker (1989a) model with an uncorrelated random field of heterogeneous bank erodibility and produced something like compound bends, but these bend shapes did not evolve from simple bends by the mechanism observed by Brice (1974) and shown in Figure 1. Tao Sun and others (T. Sun, personal communication, 2000) have recently modeled meandering near the resonance between forced and alternate bars to produce long bends that divide into smaller ones, but the simulated phenomenon lacks the double heading characteristic of most compound bend formation and noted by previous authors.

We hypothesize that this phenomenon emerges from first-order, inherent dynamics, particularly from the interactions between the flow and banks. A field study by Thorne and Furbish (1995) showed that removing the roughness of natural banks has a large and measurable effect on the dynamics of the high-velocity core of the flow in the channel. The interaction between the core and the bank produces the shear stress that erodes the bank. Previous modelers have often made the simplifying assumption that bank shear stress is proportional to the near-bank downstream velocity perturbation but have found the problem of the bank's influence, in turn, on the near-bank, shear stress-producing flow intractable (e.g., Johannesson and Parker, 1989a; Smith and McLean, 1984; Nelson and Smith, 1989b). We address this issue with a simple conceptual model.

The complicated processes of channel and landscape evolution are commonly represented by simple models that are based on both the process physics and a set of rules. For example, the cellular braided-stream model of Murray and Paola (1994, 1997), the alluvial basin model of Paola *et al.* (1992), and the landscape evolution models developed by many authors, e.g., Willgoose *et al.* (1991), Howard (1994), and Tucker and Slingerland (1994), all combine physics and rules to describe complex systems. A main objective of such modeling is to enhance our understanding of natural phenomena rather than to develop fully descriptive theories.

In this paper, we develop a simple model of river meandering that also combines physics and rules. It is based on the concept of topographic steering (Dietrich and Smith, 1983). The model treats the flow's interaction with the bank through an independent, adjustable parameter and is sufficient to produce realistic meandering (i.e., it provides "sufficient conditions for meandering" as in Howard and Knutson (1984)). We justify the model with this sufficiency. Our goal is to simulate realistic meandering over times appropriate for landscape evolution, not to perform a rigorous, physical derivation. The model produces cumuliform shapes and compound bends without invoking heterogeneity or other second-order effects.

## MODEL

In nearly all models of meander migration, local migration depends on upstream conditions, usually planform curvature. This is true of both the kinematic models of, e.g., Beck (1984), Ferguson (1984), Howard and Knutson (1984), and Furbish (1991) and the physical models of, e.g., Johannesson and Parker (1985, 1989a,b,c). In the model presented here, local migration also depends on upstream conditions, but here that condition is the shoaling driven by changing bed topography and, ultimately, changing planform curvature.

Also as in previous models, we assume that migration is equivalent to bank erosion on one side of the channel, i.e., that deposition “keeps up” with erosion.

Field studies have shown that the primary downstream current erodes the bank when the flow’s high velocity core nears the bank (e.g., Hasegawa, 1989; Pizzuto and Meckelnburg, 1989). Secondary flows “steer” the high velocity core by effecting a lateral transfer of downstream momentum. Dietrich and Smith (1983) found in a natural channel that the largest lateral transfer of downstream momentum was related to bed topography and called this phenomenon “topographic steering”. Smith and McLean (1984) showed analytically that topographic steering terms in the momentum equations were too large to be treated as perturbations, in contrast to Johannesson and Parker (1989a,b,c), who treated all secondary flows as perturbations on the mean behaviour. Our river meandering model is based on a simplified representation of the topographic steering mechanism.

We begin by estimating the lateral flow acceleration due to bed topography. We conceptualize the channel as a series of cross-sections separated by downstream incremental distances,  $ds$ , and each cross-section divided into two half-sections (Figure 2). As in most river meandering models, the bed topography is represented by a transverse bed slope at each cross-section. Where the transverse bed slope increases from one cross-section to the next, the cross-sectional area of the inner (point bar side) half-channel decreases. This decrease necessitates downstream and lateral flow accelerations. For simplicity, we neglect the downstream acceleration. We estimate the lateral unit discharge, i.e., the product of flow velocity and depth, at the channel centerline ( $n = 0$ ) due to changing bed topography in the downstream direction from continuity and by assuming a uniform downstream velocity field and a straight channel:

$$q_n = -U \frac{dA_{cs}}{ds} \quad (1)$$

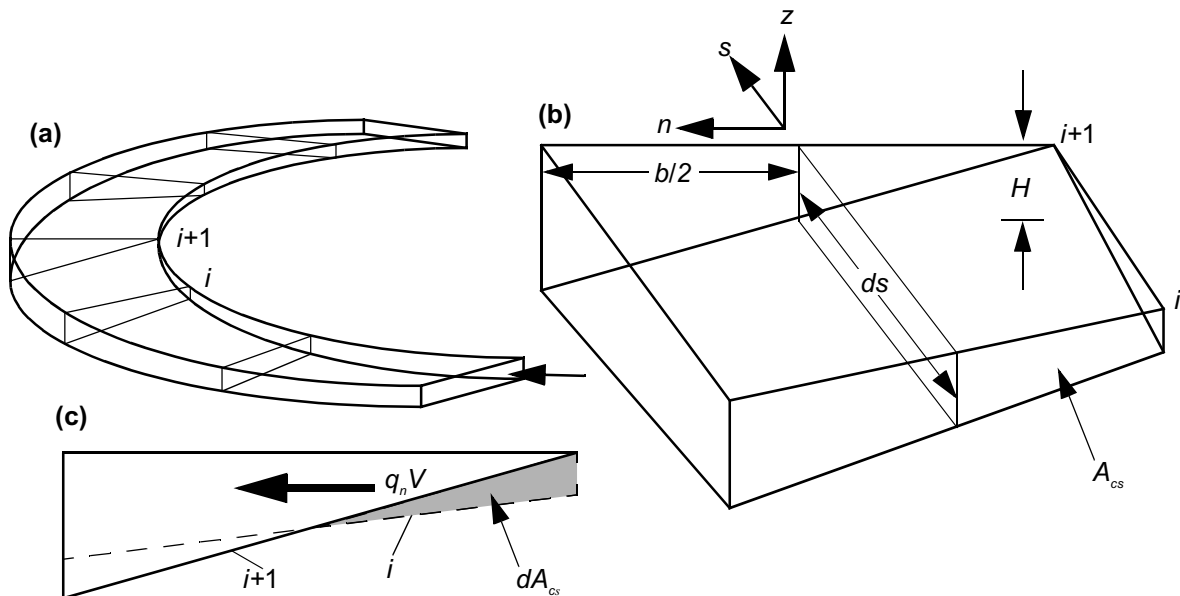


Figure 2. (a) The channel is conceptualized as a series of idealized cross-sections, e.g.,  $i$  and  $i+1$ . (b) We employ a curvilinear coordinate system as shown. Each cross-section has an average depth,  $H$ , and is divided into two half-sections of width,  $b/2$ , and successive sections, e.g.,  $i$  and  $i+1$ , are separated by an incremental downstream distance,  $ds$ . The cross-sectional area of the inner half-channel, i.e., for  $n < 0$ , is  $A_{cs}$ . (c) The change in half-channel cross-sectional area between sections, e.g.,  $i$  and  $i+1$ , is  $dA_{cs}$ . A lateral momentum transfer,  $q_n V$ , results from the downstream rate of change of the inner half-channel cross-sectional area,  $dA_{cs}/ds$

where  $U$  is the average downstream flow velocity (downstream discharge and channel width are constant and given as input parameters; downstream velocity and flow depth are determined by continuity and the Manning equation); and  $A_{cs}$  is the inner half-channel ( $n < 0$ ) cross-sectional area (Figure 2). In calculating  $A_{cs}$ , we assume that lateral and downstream variations in free surface elevation are negligible relative to lateral and downstream variations in bed elevation. Field data support this assumption (e.g., Dietrich and Whiting, 1989). The uniform downstream velocity assumption is a gross simplification of the flow field but is used here only to estimate the lateral discharge. This assumption would cause over-estimation of  $q_n$  if the flow accelerated over the point bar. Field evidence, however, indicates that the flow over the point bar actually decelerates (Dietrich and Smith, 1983). Thus, our uniform downstream velocity assumption should actually result in under-estimation of  $q_n$  by Equation (1). The straight channel assumption will lead to greater over-prediction of the lateral discharge for greater channel curvature. The lateral unit discharge, or the discharge per unit downstream distance, is positive when  $A_{cs}$  is decreasing downstream. At the channel centerline ( $n = 0$ ) the depth-averaged lateral velocity is

$$V = -\frac{U dA_{cs}}{H ds} \quad (2)$$

where  $H$  is the average flow depth and the depth at the centerline (Figure 2b). The magnitude of the force increment associated with the lateral transfer of downstream momentum from the inner to the outer half-section over an incremental downstream distance,  $ds$ , is

$$dF_n = \rho q_n V ds \quad (3)$$

where  $\rho$  is the water density, and the force increment is parallel to the  $n$ -axis. Substituting Equations (1) and (2) into Equation (3), we re-write the lateral force increment as

$$dF_n = \frac{\rho U^2}{H} \left( \frac{dA_{cs}}{ds} \right)^2 ds \quad (4)$$

Field observations by Dietrich and Smith (1983) and Dietrich and Whiting (1989) indicate that this topographic steering effect is most important for the shallower flow over the point bar, i.e., as the transverse bed slope is increasing in magnitude downstream. Where the pool is becoming shallower but the flow is still deep, i.e., transverse bed slope is decreasing in magnitude downstream, downstream acceleration of the flow is most important. Therefore, we only calculate  $dF_n$  where the magnitude of the transverse bed slope is increasing. While forces other than that represented by Equation (4) undoubtedly affect the flow, e.g., forces associated with bed friction and helical flow, our aim is to see whether topographic steering alone is sufficient for meandering.

The lateral forcing, estimated by Equation (4), steers the high velocity core toward the bank, and the core makes its closest approach to the bank at some point downstream, i.e., after some downstream lag. Where the core nears the bank, the lateral gradient of downstream velocity and, thus, the shear stress at the bank increase. Any large gradient and, thus, bank shear stress are dissipated through boundary layer development and, thus, decrease in the absence of a forcing toward the bank. We assume that the bank shear stress may be calculated from the lateral forcing of Equation (4) because this forcing pushes the high velocity core against the bank. To incorporate Equation (4) in a river meandering model, we must represent both the downstream lag and the dissipation of the force through bank shear stress. We approximate the downstream lag by finding the downstream distance traveled by a particle moving from one side of the channel to the opposite bank at the lateral and downstream velocities, or

$$L = \frac{UB}{V} \quad (5)$$

where  $B$  is

$$B = \frac{b}{2} + \frac{2A_{cs}}{H + h_i} \quad (6)$$

where  $h_i$  is the depth at the inner bank. The second term on the right hand side of Equation (6) leads to smaller  $B$  when the transverse bed slope is larger and  $B = b$  when the bed is flat, i.e.,  $h_i = H$ .

We represent the dissipation at the bank by spreading the force over the bank's area. This spreading is uniform vertically, i.e., we divide by the bank height, and Gaussian up- and downstream. We find the bank shear stress at a point along the channel,  $s$ , by summing the contributions from force increments generated at upstream points,  $s'$ :

$$\tau_w(s) = \frac{\sum_{s'} \exp\left[\frac{-(s - (s' + L(s')))^2}{2\lambda^2}\right] dF_n(s')}{\sqrt{2\pi}\lambda H} \quad (7)$$

where  $\lambda$  is the shape parameter of the Gaussian function (or the standard deviation for a Gaussian probability distribution); we use the average flow depth,  $H$ , for the bank height for simplicity; and we use a summation rather than an integral to emphasize our rules-based, numerical approach rather than continuum mechanics. According to Equation (7), each lateral force increment,  $dF_n(s')$ , is modified by a Gaussian function centered about a point that is downstream of its generation point,  $s'$ , by the lag distance,  $L(s')$ . The Gaussian is appropriate because it represents the increasing bank shear stress as the high velocity core moves toward the bank and the decreasing bank shear stress as the lateral gradient of downstream velocity decreases downstream. Thus,  $\lambda$  is like a "dissipation length scale". This dissipation length scale parameterizes bank roughness: where bank roughness is larger, lateral force increments are dissipated over a smaller distance, and therefore  $\lambda$  should be smaller. Thorne and Furbish (1995) found that, when the outside bank of a sharply curved meander bend was changed from rough to smooth, the part of the bend experiencing near-bank high velocity flow was extended both upstream and downstream. They found some additional effects of bank roughness change, but for the purposes of our simple model our choice of a dissipation length scale parameterizing bank roughness seems reasonable in light of these results. Note that this parameterization of bank roughness allows the lag distance and the dissipation length scale ( $L$  and  $\lambda$ , respectively) to vary independently.

Bank erosion and, thus, channel migration rate,  $\zeta$ , is proportional to the bank shear stress,  $\tau_w$  (positive on the left bank, negative on the right), and perpendicular to the downstream flow direction:

$$\zeta = E\tau_w\hat{n} \quad (8)$$

where  $E$  is the bank erodibility coefficient; and  $\hat{n}$  is the unit vector perpendicular to the downstream direction (Figure 2b).

Equations (4) and (6) require knowledge of the bed topography. Most river meandering models represent the bed topography by a transverse bed slope. Some models (e.g., Johannesson and Parker, 1989a; Seminara and Tubino, 1992) solve the fully coupled flow and sediment transport equations for bed topography. Others, including Ikeda (1989) and Odgaard (1982, 1986), approximate bed topography by finding the equilibrium slope needed to balance the force of gravity and the shear stress of the secondary helical, or curvature-induced, flow on the grains at the bed. We follow the latter approach.

Ikeda's (1989) formula for the transverse bed slope, evaluated at the channel centerline, is

$$S_T = KHC \quad (9)$$

$$K = \sqrt{\frac{\Psi}{\Psi_{cr}} \left( \frac{0.2278}{\sqrt{C_f}} - 0.3606 \right)} \quad (10)$$

where  $C$  is channel centerline curvature;  $\Psi$  and  $\Psi_{cr}$  are dimensionless shear stress and critical shear stress, respectively; and  $C_f$  is the friction factor. Ikeda's formula is appropriate for gravel-bed channels. For sand-bed channels, we have modified Ikeda's formula to account for the effect of form drag (Engelund and Hansen, 1967). The modified form of Equation (10) is

$$K = \frac{\Psi'}{\Psi} \sqrt{\frac{\Psi'}{\Psi_{cr}}} \left[ \frac{0.2278}{\kappa} \ln \left( \frac{11.0 \Psi' H}{\Psi d_{50}} \right) - 0.3606 \right] \quad (11)$$

where  $\Psi'$  is dimensionless skin friction;  $\kappa$  is von Karman's constant (=0.4); and  $d_{50}$  is the median bed material grain diameter (Lancaster, 1998). The above form is used in the simulations presented herein.

We used data from Muddy Creek, Wyoming (Dietrich and Smith, 1983, 1984; Dietrich and Whiting, 1989), for the model parameter set (Table I) and testing of the transverse bed slope model. The transverse bed slope predicted by Equations (9) and (11) is compared to cross-sections measured by Dietrich and Smith (1983) in Figure 3. Ikeda's (1989) unmodified formula, i.e., Equation (10), predicted a transverse bed slope approximately twice as large. We predict the same transverse bed slope for each of the three sections because the curvature is the same at each. In reality, the transverse bed slope seems to "lag" behind the prediction such that the predicted slopes are too large for the first two sections (see Zhou *et al.*, 1993, for a prediction of this "phase lag"). Johannesson and Parker (1989c) used an effective curvature that integrated contributions from upstream to account for this lag. Typically, this lag is quite small, and, for our simple model, such complication is probably unwarranted.

Our solution for the transverse bed slope is most accurate at the channel centerline and least accurate at the banks, and this error is larger for larger transverse bed slopes. Ikeda (1989) solved for the bed topography over the entire channel width and showed that the transverse bed slope is lower over the point bar and in the deepest part of the pool, especially when grain size is allowed to vary laterally. For large transverse bed slopes we constrain the bed topography by "chopping off" any part of the bed that would rise above the free water surface and, to keep the cross-sectional area constant, any part of the pool that would sink below twice the average depth (Figure 4a). These constraints are arbitrary but effectively limit the error for large transverse bed slopes, i.e.,  $S_T > 2H/b$ .

When Equations (4), (9), and (10) are applied to an ideal, sine-generated channel centerline, the lateral force increment's maximum magnitude is similar to that of the bottom shear stress integrated over a channel increment (Lancaster, 1998). This result is consistent with the findings of Dietrich and Smith (1983) and Dietrich and Whiting (1989) that these two forces are of similar magnitude and indicates that our representation of the lateral forcing is accurate to within an order of magnitude.

We use a finite difference method to solve for the lateral migration (Equation 8) at discrete points along a

Table I. Default parameter values used in model simulations<sup>a</sup>

Parameter	Value
Discharge, m <sup>3</sup> /s	1.6
Channel width, $b$ , m	5.5
Average depth, $H$ , m	0.5
Manning roughness	0.036
Median grain size, $d_{50}$ , mm	0.7
Channel slope	0.0014
Valley slope	0.0021
Radius of curvature, $1/C$ , m	8.0
Dissipation scale, $\lambda$ , m	8.0
Nominal discretization, $\Delta s$ , m	2.8

a. Discharge, width, roughness, grain size, and valley slope are held constant during the simulation; depth, channel slope, and radius of curvature are given for reference. All parameters except the dissipation scale,  $\lambda$ , and the nominal discretization,  $\Delta s$ , are derived from the Muddy Creek, WY, data published by Dietrich and Smith (1983, 1984) and Dietrich and Whiting (1989).

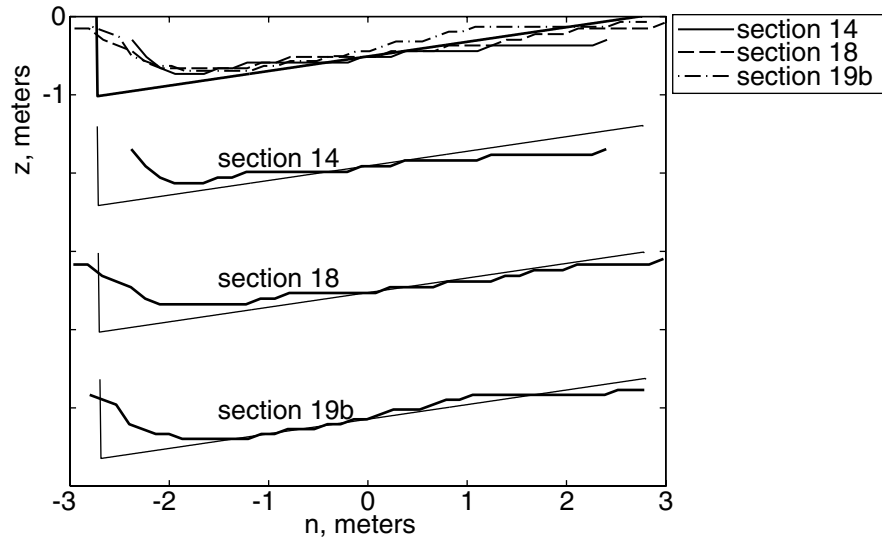


Figure 3. Comparison of observed and predicted bed topographies for Muddy Creek channel cross-sections measured by Dietrich and Smith (1983). Section number is increasing downstream, and all three are in the same bend. Radius of curvature at the three sections and used in the prediction is from Table I

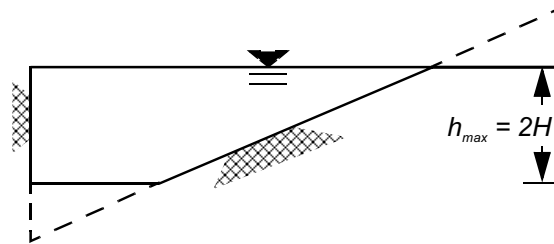


Figure 4. Illustration of constraints on bed topography for large transverse bed slope

stream reach. Initially, the distance between channel points is the nominal discretization (Table I). As the channel points move apart, new points are added between any two points when they are farther apart than twice the nominal discretization. This scheme should result in an average discretization of 1.5 times the nominal value. The initial stream in the examples presented in this paper is small-amplitude brown noise in a nearly straight line down the valley axis (see, e.g., Howard and Knutson, 1984). Discharge, roughness, grain size, width, and valley slope are input parameters and are constant in both space and time (Table I). Channel slope is constant in space but changes in time with the sinuosity.

An example of model meander evolution for short time and channel length is shown in Figure 5. The model meander bends appear realistic in their form and behaviour: small bends migrate downstream, larger bends migrate laterally, and one bend becomes compound in the penultimate time slice. As we will show in a later section, such compound bends may separate into distinct bends and lead to multi-bend loop formation.

## ANALYTICAL METHOD

We present here a new sinuosity-based method for analyzing planforms of meandering channels. Channel sinuosity is usually presented as a single number, but the value of that number will vary with measurement

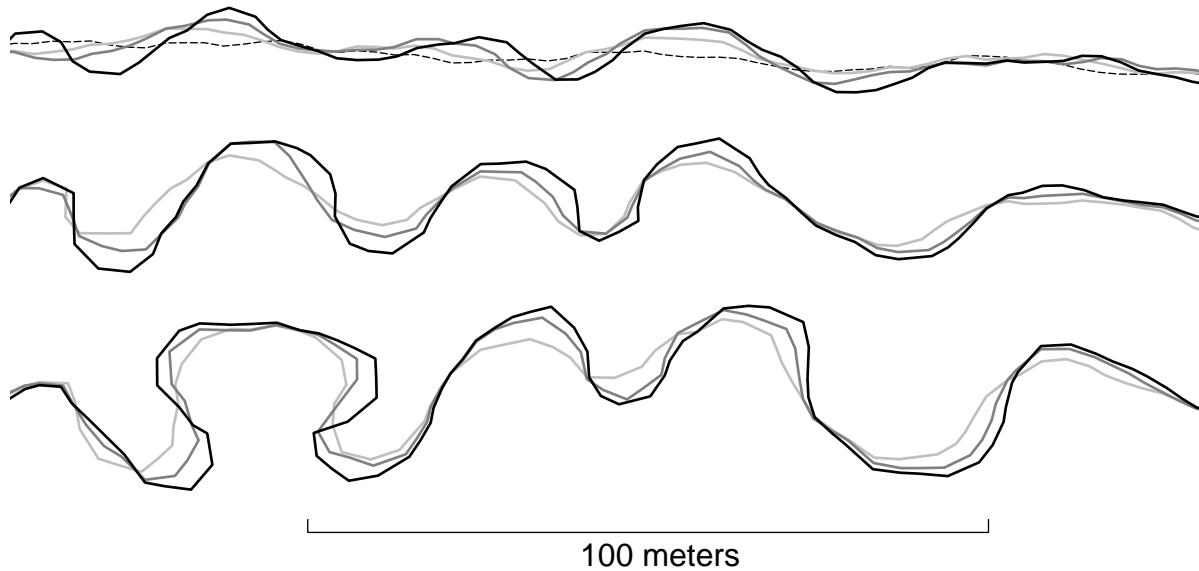


Figure 5. Meander evolution with default parameters (Table I) except for  $\lambda=4m$  for a total of 1 time unit. Channels are shown every 0.1 time unit, and several time slices are overlain. The first time is shown as a dashed line. Subsequent times are shaded triplets where darker is later

location and channel length. Howard and Hemberger (1991) introduced statistics for measuring contributions to sinuosity at different length-scales, the half-meander, full-meander, and residual sinuosities, while Andrieu (1994, 1996) developed a method for identifying multiple scales of planform curvature. Our new method measures the average sinuosity and its variability over the whole possible range of lengths for a given reach. Objective criteria then identify particular channel lengths at which contributions to sinuosity are important and what those contributions are.

For every pair of points along a discretized channel both the downstream distance,  $s'$ , and the straight-line distance,  $r$ , between the points are measured. The ratio of these distances is the sinuosity. These sinuosity measures are binned according to channel length,  $s'$ , and the mean and variance of the measures in each bin are calculated. We may, then, express the bin means and variances as functions of channel length,  $s'$ :

$$\mu_s(s') = \left\langle \frac{s'}{r(s, s+s')} \right\rangle \tag{12}$$

$$\sigma_s^2(s') = \left\langle \left( \frac{s'}{r(s, s+s')} - \mu_s(s') \right)^2 \right\rangle \tag{13}$$

where  $s'$  is the length of the channel segment;  $r(s, s+s')$  is the straight-line distance between the segment's end points at  $s$  and  $s+s'$ ; and the angle brackets indicate the expected value for all possible values of  $s$ . To facilitate comparisons across different stream sizes, we normalize the  $s'$ -axis by mean channel width. The mean sinuosity,  $\mu_s$ , should generally increase with increasing  $s'$ , from unity for adjacent points to the total reach sinuosity. This increase may not be monotonic because of the statistical nature of the quantity, but it will be nearly monotonic.

For a random walk, allowed to cross itself and with no characteristic length scale governing its course, sinuosity mean and variance increase as power laws of  $s'$  until  $s'$  approaches the total walk length. For a meandering channel with a characteristic length or lengths, the sinuosity mean and variance will reveal those lengths and their importance to planform sinuosity, as we will show in the next section.

The next step in the analysis involves objective identification of characteristic lengths. As the measurement length increases and approaches the length of single bends, the mean sinuosity increases, and the rate

of its increase also increases because typical channel segments tend to curve back on themselves as measurement length increases. As measurement lengths surpass the typical bend length, mean sinuosity may continue to increase, but the rate decreases because at least some channel segments stop curving back on themselves. The length of simple bends,  $s'_{sb}$ , will be identified by that decrease in slope. At greater lengths many measurements will have moderate sinuosity and encompass more than one bend, but some measurements will encompass longer, particularly sinuous bends and loops that will weight the mean toward larger values and make the sinuosity variance large. At such lengths there will be peaks in  $\sigma_s^2(s')$  and, possibly, corresponding inflections in  $\mu_s(s')$ . The first such peak in  $\sigma_s^2(s')$  will identify the length,  $s'_{v1}$ . This length will likely be that of particularly long simple or compound bends. If the first peak in  $\sigma_s^2(s')$  is not the largest, then the largest peak in  $\sigma_s^2(s')$  will identify a length we will call  $s'_{v2}$ . Otherwise  $s'_{v2}$  will be identified by the next-largest peak in  $\sigma_s^2(s')$ . This last length,  $s'_{v2}$ , will likely correspond to multi-bend loops that make important contributions to total sinuosity. The lengths defined above represent a simple and objective set of criteria for determining characteristic length-scales. Plots of mean sinuosity at each length versus the lengths themselves will facilitate comparison among planforms and detection of similar, or dissimilar, features. In order to determine what the above lengths represent, we will find examples of planform features, such as individual bends, that have the same length as the identified length-scales.

### ANALYSIS OF NATURAL CHANNELS

The natural channels analyzed are listed in Table II and shown in Figure 6. We selected reaches of Alaskan streams that are: (i) single-threaded, i.e., not braided; (ii) intensely meandering; and (iii) unconfined by terraces or valley walls. The channel centerlines were digitized by hand from topographic maps. To eliminate errors and bias, we corrected the digitizations by visually comparing the digitized and mapped planforms and moving or deleting points as necessary. We measured channel width at many locations ( $N > 50$ ) along each reach from the topographic maps with the digitizer and calculated the mean and standard deviation of those measurements (Table II).

The results of the sinuosity analysis are shown in Figures 7, 8, and 9 and Table III. The sinuosity means and variances are plotted versus the normalized length of the measurement in Figure 7, and the points,  $\mu_s(s'_{sb})$ ,  $\mu_s(s'_{v1})$ , and  $\mu_s(s'_{v2})$ , are also shown. Noteworthy features of these plots are the breaks in, or leveling off of, increasing mean sinuosity with increasing reach length, often more than one for a stream reach. The lengths where these breaks occur correspond to peaks in sinuosity variance. Thus, by using the  $\sigma_s^2$  peaks as indicators of characteristic lengths, we are finding lengths demarcating breaks in increasing  $\mu_s$ . In other

Table II. Meandering stream reaches

Stream reach	Quadrangle map(s) (all AK)	Mean channel width $\pm \sigma$ , meters	Reach length, channel widths
Preacher Creek (PC)	Ft. Yukon (A-2)	$31.2 \pm 7.0$	1300
Takotna River (TAR)	Iditarod (C-2)	$33.9 \pm 12.0$	650
North Fork Kuskokwim River, McKinley (KRMC)	Mt. McKinley (D-6)	$38.3 \pm 7.4$	460
Melozitna River (MR)	Melozitna (B-3)	$46.2 \pm 16.0$	990
Teklanika River (TER)	Fairbanks (B-5, B-6)	$48.0 \pm 16.6$	1100
Dishna River (DR)	Ophir (C-3)	$50.4 \pm 13.7$	510
Birch Creek (BC)	Ft. Yukon (A-2)	$57.7 \pm 14.1$	1160
North Fork Kuskokwim River, Medfra (KRME)	Medfra (B-2, B-3)	$95.5 \pm 24.1$	380
Innoko River (IR)	Ophir (C-3)	$113.0 \pm 18.0$	370

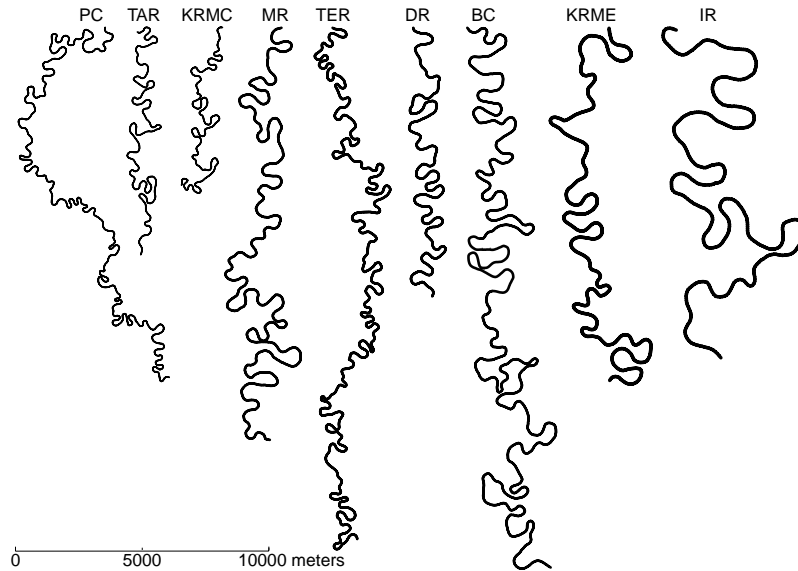


Figure 6. Meandering Alaskan streams used in the analysis. Flow is from top to bottom

Table III. Summary of natural stream analysis: lengths, in channel widths, and mean sinuosities at those lengths

Stream reach	$s'_{sb}$	$\mu_s(s'_{sb})$	$s'_{v1}$	$\mu_s(s'_{v1})$	$s'_{v2}$	$\mu_s(s'_{v2})$
PC	19	1.6	26	1.9	91	2.3
TAR	19	1.5	33	2.1	78	2.7
KRMC	18	1.7	31	2.3	120	2.8
MR	23	1.5	40	2.2	120	3.0
TER	13	1.6	23	2.1	80	2.5
DR	22	1.7	45	2.5	73	2.6
BC	19	1.5	33	2.1	91	3.3
KRME	11	1.4	28	2.4	44	2.5
IR	18	1.5	36	2.4	120	3.5

words, these lengths represent important contributions to planform sinuosity.

The mean sinuosity at the three identified channel lengths,  $s'_{sb}$ ,  $s'_{v1}$ , and  $s'_{v2}$ , for all the channels are plotted as  $\mu_s(s'_{sb})$ ,  $\mu_s(s'_{v1})$ , and  $\mu_s(s'_{v2})$  in Figure 8 and tabulated in Table III. This plot shows that all three sets of points fall in distinct clusters. The smallest lengths,  $s'_{sb}$ , and corresponding mean sinuosities are most tightly clustered:  $11 \leq s'_{sb} \leq 23$  channel widths; and  $1.4 \leq \mu_s(s'_{sb}) \leq 1.7$ . Next, the points corresponding to intermediate lengths,  $s'_{v1}$ , are less tightly clustered:  $23 \leq s'_{v1} \leq 45$  channel widths; and  $1.9 \leq \mu_s(s'_{v1}) \leq 2.5$ . Finally, the longest lengths,  $s'_{v2}$ , are least tightly clustered:  $44 \leq s'_{v2} \leq 120$  channel widths; and  $2.3 \leq \mu_s(s'_{v2}) \leq 3.5$ .

Representative parts of the channels corresponding to the lengths,  $s'_{sb}$ ,  $s'_{v1}$ , and  $s'_{v2}$ , are shown for two of the reaches, KRMC and MR, in Figure 9, which shows that, for these two streams,  $s'_{sb}$  does, as predicted, correspond to the typical length of simple bends;  $s'_{v1}$  corresponds the length of long, often compound, bends; and  $s'_{v2}$  corresponds to the length of multi-bend loops, as with KRMC, or particularly sinuous bend sequences that may include multi-bend loops, as in MR.

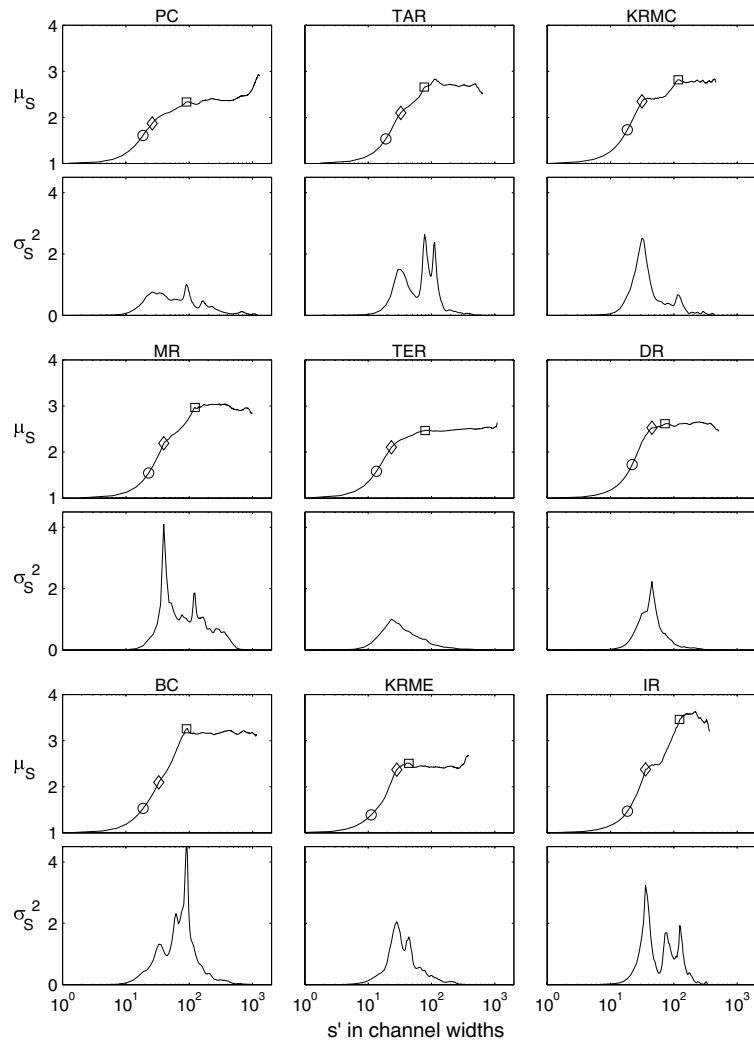


Figure 7. Sinuosity mean and variance versus normalized reach length for the meandering streams listed in Table II and shown in Figure 6. Mean sinuosity versus length-scales, i.e.,  $\mu_s(s'_{v2})$ ,  $\mu_s(s'_{v1})$ , and  $\mu_s(s'_{vb})$ , are also shown as open circles, diamonds, and squares, respectively

Note that the relative importance of the contributions to sinuosity at the three lengths varies among streams (Figure 7). In fact,  $\mu_s(s'_{v2})$  differs only slightly from  $\mu_s(s'_{v1})$  for three of the natural streams, TER, DR, and KRME, and for two of those, TER and DR, the choice of  $s'_{v2}$  is relatively arbitrary. This fact indicates significant natural variation in the importance of multi-bend loops to planform complexity.

## MODEL RESULTS AND ANALYSIS

Channels simulated with the model of Johannesson and Parker (1989c) (JP model) (see appendix) are shown in Figure 10. Analysis of these simulated planforms is shown in Figures 11 and 12 and tabulated in Table IV. The mean sinuosity lacks the multiple prominent breaks that were found for the natural channels but does have some breaks in its rate of increase with measurement length. These slope breaks correspond to peaks in

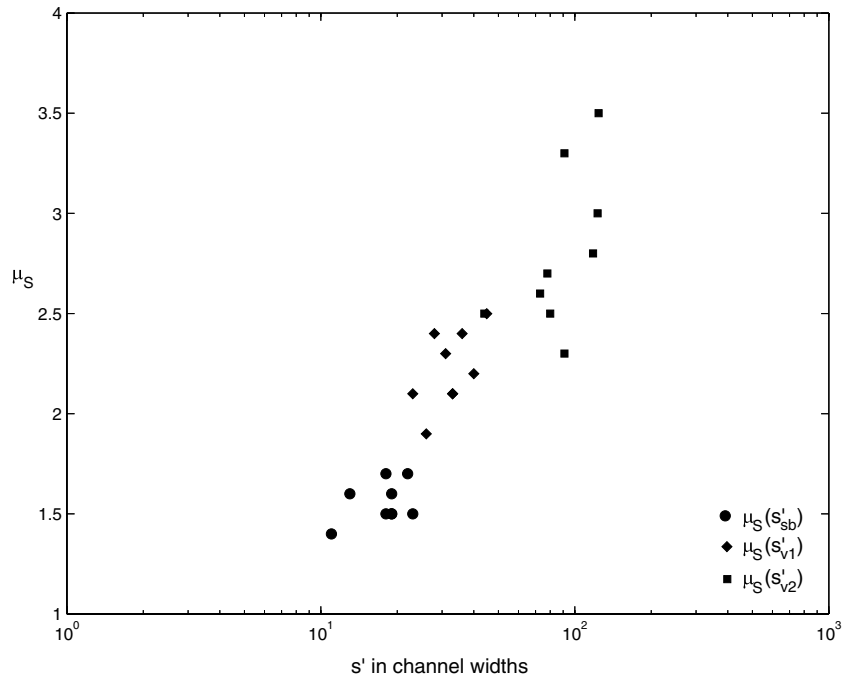


Figure 8. Mean sinuosity versus length-scales of first  $\mu_s$  slope decrease, first  $\sigma_s^2$  peak, and largest or next-largest  $\sigma_s^2$  peak for natural channels

the sinuosity variance, as with the natural channels. For the most part, points for the three lengths and corresponding mean sinuosities are clustered, as in the natural channels. One of the  $s'_{sb}$  points has significantly higher length and sinuosity than the others. This point is for the first time slice, before cut-off for many of the first “generation” of bends, and, so, the channel is especially sinuous at this time, and most of the bends are long. At subsequent times the points are clustered at sinuosities similar to the corresponding points for the natural channels but shorter lengths. Points corresponding to  $s'_{v1}$  are clustered at lengths similar to natural channels but higher sinuosity. Points corresponding to  $s'_{v2}$  have sinuosities similar to natural channels but shorter lengths. Note that difference between model and natural  $s'_{v2}$  values is much greater than the difference between model and natural  $s'_{sb}$  values. Comparison of Figures 9 and 10 reveals that features corresponding to  $s'_{v2}$  are different in these natural and simulated channels:  $s'_{v2}$  for the natural channels corresponds to multi-bend loops or sequences of bends;  $s'_{v2}$  for the JP model channels corresponds to long, sinuous, single bends.

Simulated channel evolution with the new model and default parameters (Table I) is shown in Figure 13. The model produces complicated meandering patterns that resemble natural forms. Specifically, the model produces simple and compound bends and multi-bend loops that resemble natural ones (Figure 14). Figure

Table IV. Summary of analysis of channel planforms simulated with the JP model: lengths, in channel widths, and mean sinuosities at those lengths

Time	$s'_{sb}$	$\mu_s(s'_{sb})$	$s'_{v1}$	$\mu_s(s'_{v1})$	$s'_{v2}$	$\mu_s(s'_{v2})$
20	17	2.3	21	2.7	47	2.9
40	12	1.8	21	2.5	28	2.7
60	10	1.6	30	2.8	57	3.4
80	10	1.5	28	2.6	43	3.0
100	10	1.5	32	2.7	43	3.1

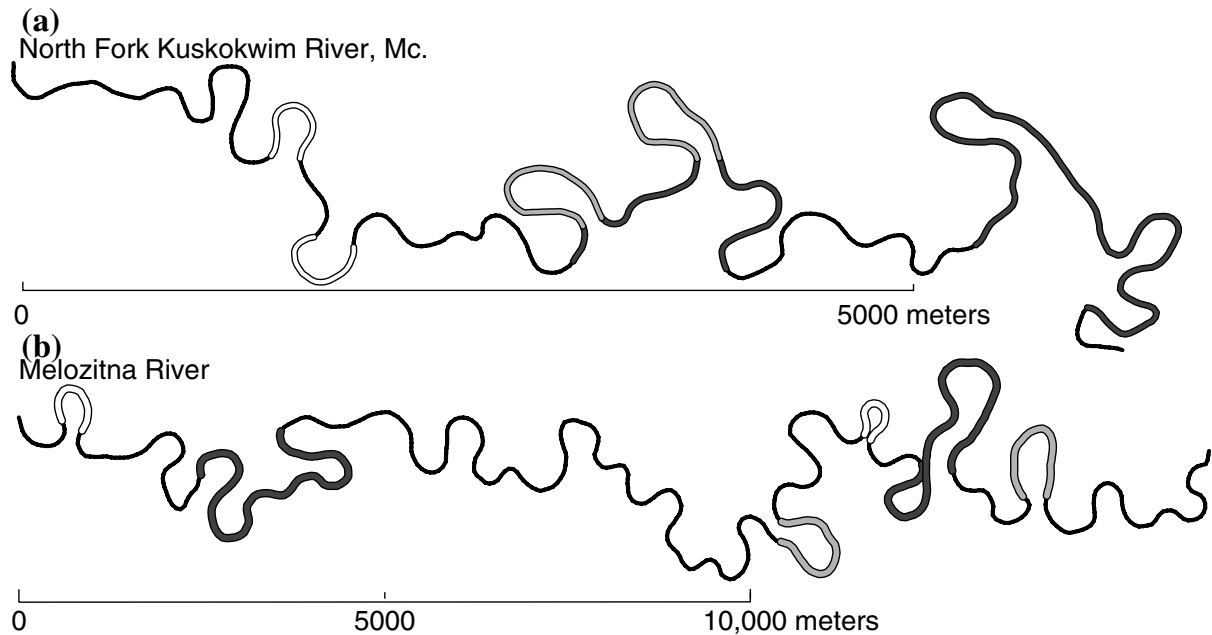


Figure 9. Illustration of the forms represented by the three channel length-scales shown in Figure 8 and Table III for two of the Alaskan stream reaches, (a) North Fork Kuskokwim River, McKinley, and (b) Melozitna River. Filled regions with different shades correspond to the three channel length-scales (Figure 8): white is  $s'_{sb}$ , light gray is  $s'_{v1}$ , and dark gray is  $s'_{v2}$

15 shows the sinuosity mean and variance for these model channels. Total sinuosities are at the upper range of those of the natural channels. As for the natural channels,  $\mu_s$  often has multiple breaks corresponding to  $\sigma_s^2$  peaks, but these breaks in  $\mu_s$  are less well defined for the simulated channels than for some of the natural channels. As with the natural channels, points in the plot of mean sinuosities at the different lengths,  $s'_{sb}$ ,  $s'_{v1}$ , and  $s'_{v2}$ , are clustered (Figure 16 and Table V). The model  $s'_{sb}$  values are somewhat smaller than those of the natural channels, but mean sinuosities at those lengths are similar. Similarly, the model  $s'_{v1}$  values are smaller than for natural channels, but the sinuosities are similar. Interestingly, the  $\mu_s(s'_{v2})$  points fall on a distinct trend that goes through the natural  $\mu_s(s'_{v2})$  points, but the latter are arranged more nearly vertically. As stated above, it is likely that this scatter in mean sinuosity reflects natural variation in multi-bend loops' importance to planform sinuosity. The model points represent a single case, and  $\mu_s(s'_{v2})$  variation represents changes over time, not in characteristics as with the natural channels. The larger  $s'_{v2}$  values indicate that model multi-bend loops tend to get longer than natural multi-bend loops, e.g., in Figure 14(c).

Varying  $\lambda$  has a significant, visible effect on the simulated channel planforms (Figure 17). Decreasing  $\lambda$  by one-half from its default value produces a less sinuous channel planform and apparently suppresses multi-bend loops' importance to planform sinuosity (Figure 17a). There is some difference in the clustering of  $\mu_s(s'_{sb})$  and  $\mu_s(s'_{v1})$  points between these two cases, but the major difference is in the  $\mu_s(s'_{v2})$  points: the points for smaller  $\lambda$  are generally shifted back along the trend to lower lengths and sinuosities relative to the points for default  $\lambda$  (Figure 18). From this shift we infer that decreasing  $\lambda$  also decreases the importance of multi-bend loop formation to planform sinuosity, and this inference is consistent with visual assessment of the planform. Note that decreasing  $\lambda$  increases bank shear stress (Equation 7) and, thus, typical migration rates relative to the default case. We can be certain, therefore, that the smaller- $\lambda$  simulation had ample time to develop multi-bend loops if it were so inclined.

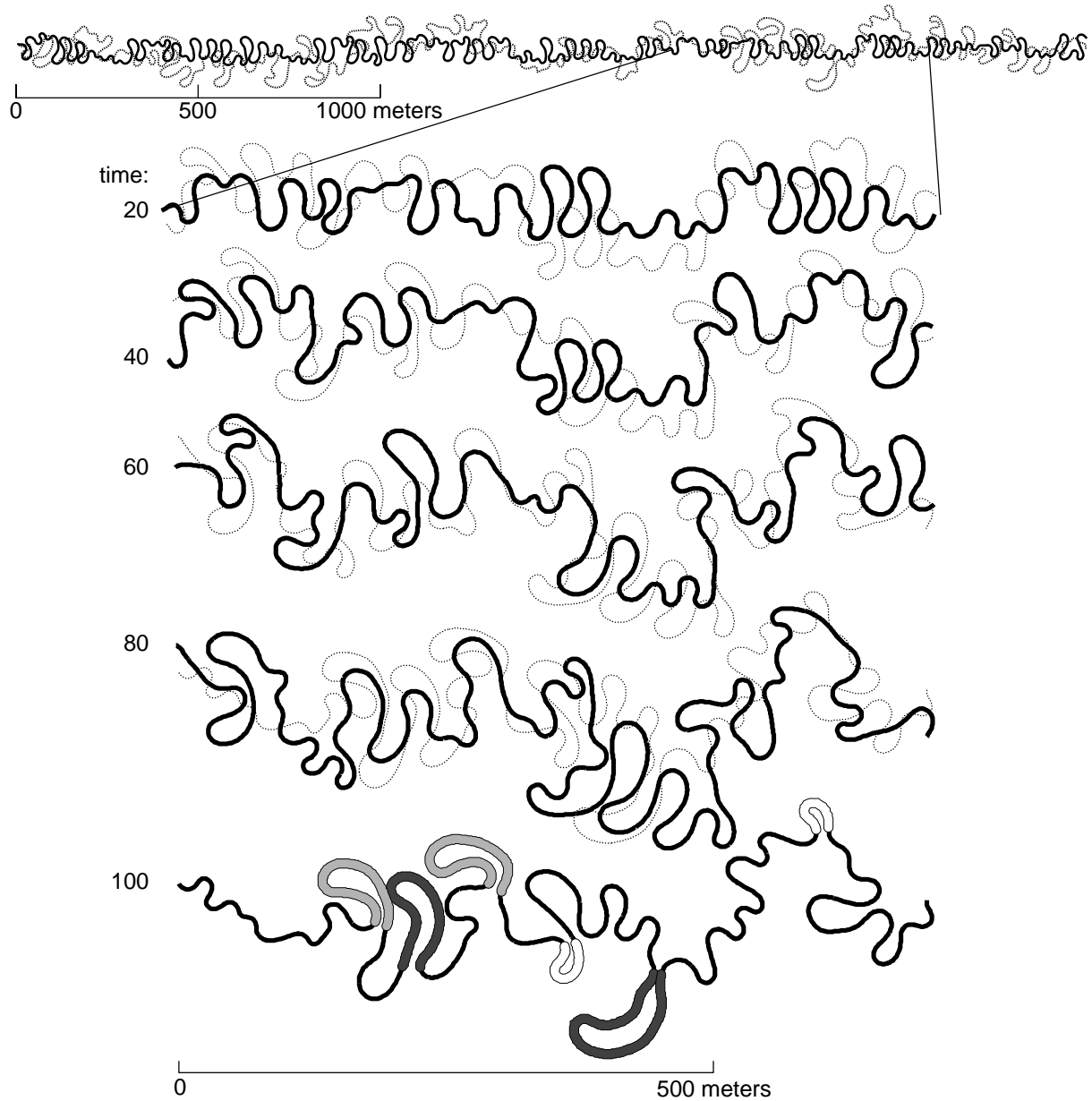


Figure 10. Simulation with the JP model and default parameters. At top, channels at 20 (solid) and 100 (dotted) time units are superimposed. Below, a part is enlarged and shown at 20, 40, 60, 80, and 100 time units, from top to bottom. For all but the last time, the next time is superimposed as a dotted line. In the last time slice, filled regions with different shades correspond to the three channel length-scales (Figure 12 and Table IV): white is  $s'_{sb}$ , light gray is  $s'_{v1}$ , and dark gray is  $s'_{v2}$

The effect of increasing  $\lambda$  by a factor of  $\sim 2$  from its default value is to make the simulated meander pattern appear unrealistic and, at later times, quite sinuous (Figure 17b). Many bends are sickle-shaped, with the convex side facing upstream. None of the natural streams in Figure 6 have bends with similar shapes, and we have not observed such shapes in nature. Mean sinuosities at the lengths,  $s'_{sb}$ ,  $s'_{v1}$ , and  $s'_{v2}$ , are also unusual (Figure 18). The  $\mu_s(s'_{sb})$  points are clustered at small lengths and sinuosities because of the prevalence of

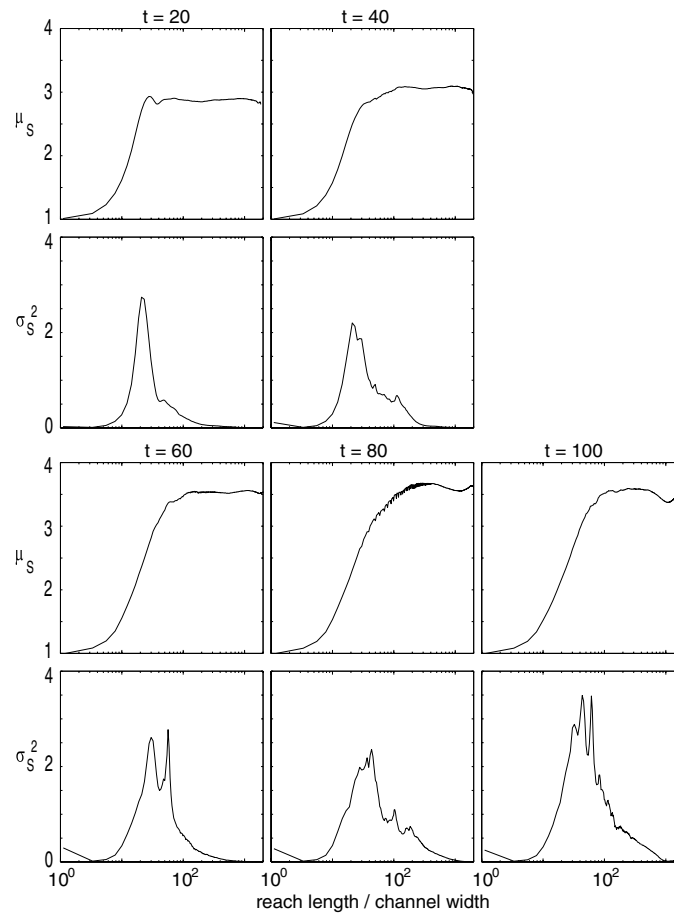


Figure 11. Analysis for simulations with the JP model and default parameters (Table I and Figure 10). Sinuosity mean and variance versus normalized reach length for the simulated channels at times 20, 40, 60, 80, and 100 model time units, as labeled

small, sickle-shaped bends. The  $\mu_s(s'_v2)$  points have widely varying sinuosities and do not generally fall along the trend of the other points. This variation is partly due to increasing sinuosity with time and the lack of a distinct second  $\sigma_s^2$  peak at the first time (Table V) because the larger  $\lambda$ -value decreases bank shear stresses (Equation 7) and, thus, migration rates relative to the other simulations.

## DISCUSSION

Our simple meandering model reproduces an observable, quantifiable phenomenon, compound bend/multi-bend loop formation. Our new sinuosity-based channel planform analysis measures the prevalence of this phenomenon in both natural and model channels. Moreover, our model predicts that a larger bank shear stress dissipation length scale, which corresponds to smoother banks, promotes compound bend formation. The mechanism by which this occurs is provided by the field experiment of Thorne and Furbish (1995), who found that smoother banks made for a larger dissipation length scale and reasoned that smoother banks should lead to more asymmetric, downstream bend migration. From observing model and natural channel evolution we have found that compound bends are usually formed in bends with a mid-bend section of low curvature when an upstream bend migrates rapidly downstream and, thus, “disturbs” the downstream bend.

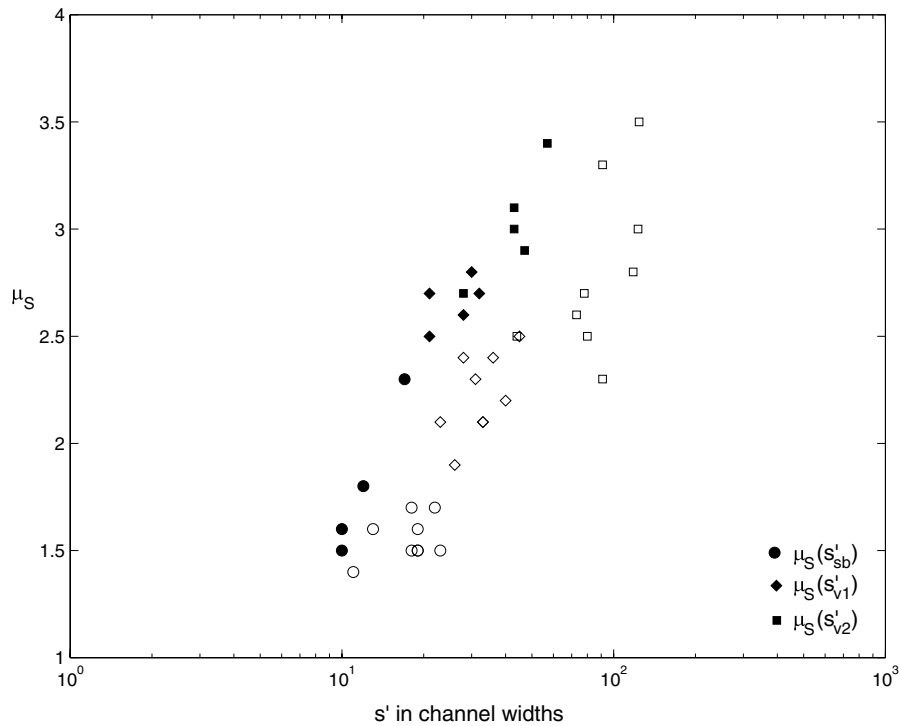


Figure 12.  $\mu_S(s'_{sb})$ ,  $\mu_S(s'_{v1})$ , and  $\mu_S(s'_{v2})$  for natural channels (open symbols) and channels simulated with the JP model and default parameters (black symbols)

This disturbance is realized in the form of a curvature reversal where it was previously small, and, thus, a compound bend is formed. This curvature reversal may then develop into a rapidly downstream migrating bend of its own. Thus, the compound bend separates and becomes a multi-bend loop. Natural and model examples of compound bend formation are shown in Figures 1 and 5, respectively. Given the findings of Thorne and Furbish (1995) and the similarity between the model and observed natural mechanisms for compound bend formation, our model provides a reasonable, qualitative picture of compound bend formation's sensitivities. A quantitative evaluation of  $\lambda$ 's variation with bank roughness is, however, beyond the scope of this work.

Both the present model and the JP model use upstream characteristics to determine migration at downstream points, but only the present model produces compound bends as described above. In the JP model, migration at a point is most strongly influenced by local curvature, and the effect of upstream points decreases downstream with a constant, uniform length scale. In the present model, migration at a point is most strongly influenced by along-stream curvature variation at some distance upstream, and the effect of that variation decreases downstream with a constant, uniform length scale. However, the distance,  $L$ , from the curvature variation to the downstream locus of its maximum effect is neither constant nor uniform but, rather, varies inversely with the magnitude of the curvature variation. A sequence of bends may be relatively stable and favor longer, slowly migrating bends until their configuration changes radically, e.g., due to a cut-off, at which point the configuration of downstream bends can destabilize in favor of smaller bends with greater magnitudes of along-stream curvature variations and, therefore, smaller downstream lags,  $L$ . Our results show that this scenario is favored when the bank shear stress dissipation length scale is larger. Recently, Tao Sun (personal communication, 2000) has modeled meander migration under conditions close to the resonance between forced and alternate bars. Under these conditions, instabilities develop that lead to compound bend formation, though not the double-heading produced by the present model and observed in

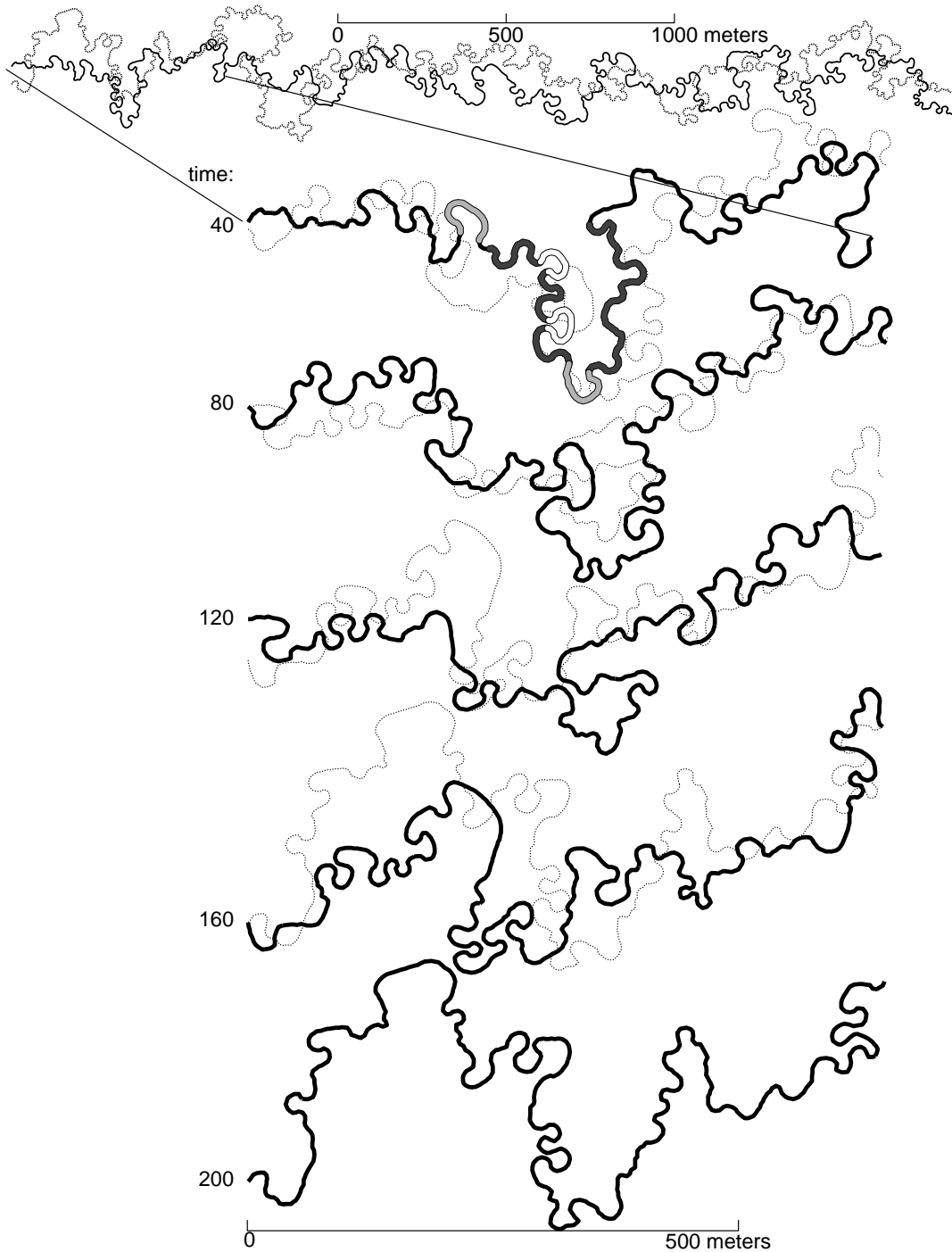


Figure 13. Simulation with default parameters (Table I). At top, channels at 40 (solid) and 200 (dotted) time units are superimposed. Below, a part is enlarged and shown at 40, 80, 120, 160, and 200 time units, from top to bottom. For all but the last time, the next time is superimposed as a dotted line. In the first time slice, filled regions with different shades correspond to the three channel length-scales (Figure 16): white is  $s'_{s,b}$ , light gray is  $s'_{v,1}$ , and dark gray is  $s'_{v,2}$

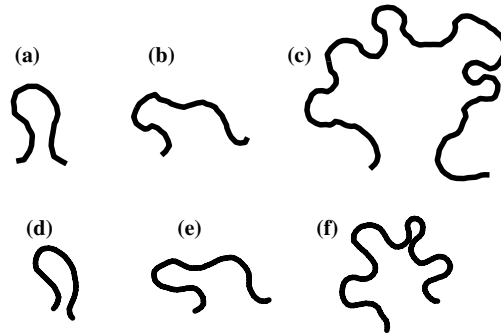


Figure 14. Examples of model channel forms from the simulation of Figure 13: (a) simple bend; (b) compound bend; and (c) multi-bend loop; and natural channel forms from the Kuskokwim and Melozitna Rivers, Alaska: (d) simple bend; (e) compound bend; and (f) multi-bend loop. Flow is from left to right.

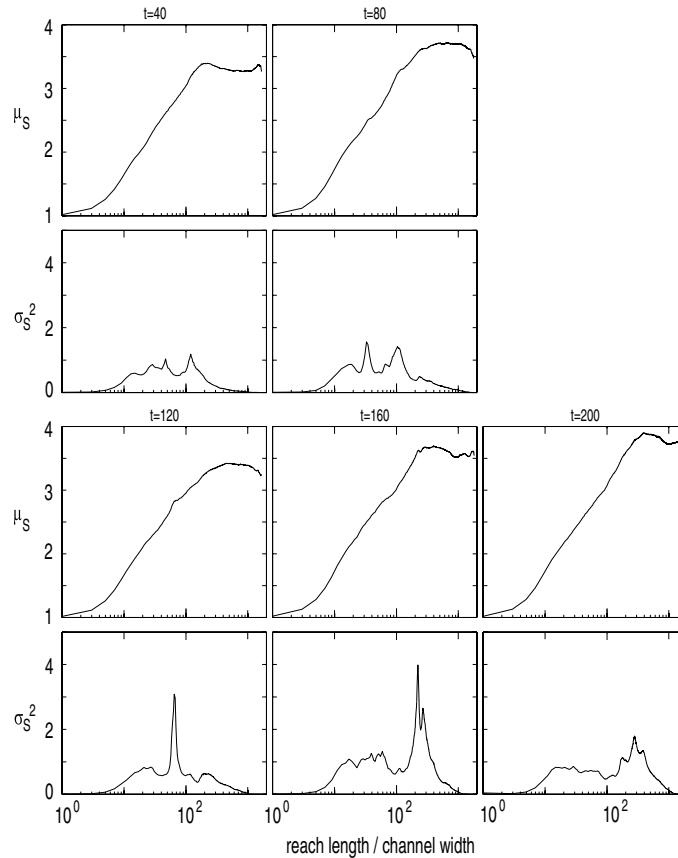


Figure 15. Analysis for simulations with default parameters (Table I and Figure 13). Sinuosity mean and variance versus normalized reach length for the simulated channels at times 40, 80, 120, 160, and 200 model time units, as labeled.

nature. We speculate that the interactions between a fixed alternate bar wavelength and a varying forced bar wavelength could lead to instabilities similar to those described above for the present model. The basic JP model presented here cannot produce these instabilities because it lacks such wavelength interactions.

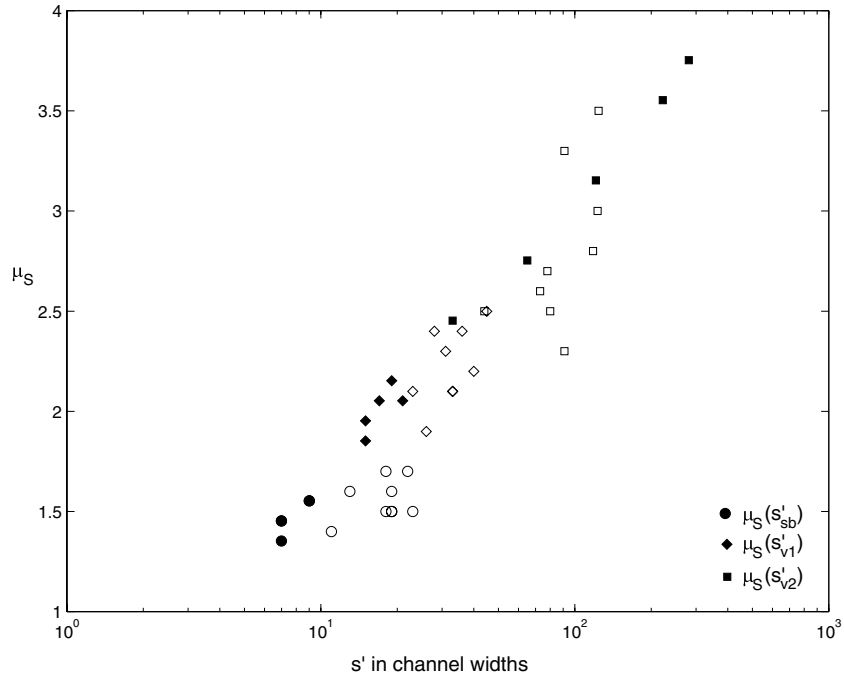


Figure 16.  $\mu_s(s'_{sb})$ ,  $\mu_s(s'_{v1})$ , and  $\mu_s(s'_{v2})$  for natural channels (open symbols) and channels simulated with default parameters (black symbols)

Table V. Summary of model stream analyses: lengths, in channel widths, and mean sinuosities at those lengths

Run	Time	$s'_{sb}$	$\mu_s(s'_{sb})$	$s'_{v1}$	$\mu_s(s'_{v1})$	$s'_{v2}$	$\mu_s(s'_{v2})$
default parameters	40	9.0	1.6	15	1.9	120	3.2
	80	7.0	1.5	19	2.2	33	2.5
	120	7.0	1.4	21	2.1	65	2.8
	160	9.0	1.6	17	2.1	220	3.6
	200	7.0	1.5	15	2.0	280	3.8
$\lambda=4.0m$	40	6.9	1.6	19	2.4	29	2.5
	80	4.9	1.4	13	2.0	23	2.4
	120	7.0	1.6	19	2.3	31	2.4
	160	4.9	1.4	27	2.5	52	2.7
	200	4.9	1.4	15	2.1	48	2.7
$\lambda=15m$	40	5.2	1.4	20	2.0	120	2.1 <sup>a</sup>
	80	5.1	1.3	20	2.0	57	2.7
	120	5.2	1.4	13	1.8	92	3.8
	160	5.2	1.4	13	1.8	80	3.4
	200	3.1	1.2	32	2.4	100	3.3

a. Not really a second peak in sinuosity variance.

Variations of parameters other than  $\lambda$  could affect the propensity for compound bend formation by changing the downstream lag,  $L$  (Equation 5). Specifically, valley slope,  $S_v$ , and bed material median grain diameter,  $d_{50}$ , affect  $L$ , and lag could be sensitive to nominal discretization,  $\Delta s$ . The sensitivity of compound bend formation to these parameters is summarized in Table VI. Compound bend formation is relatively insensitive

to changes in  $S_f$  because of the weak dependence of  $L$  on friction slope,  $S_f$ , and large variations in sinuosity and, thus,  $S_f$  over time. Likewise, transverse bed slope's sensitivity to grain size is also weak (Equation 11), and, therefore, compound bend formation's sensitivity to grain size is weak. Though the nominal discretiza-

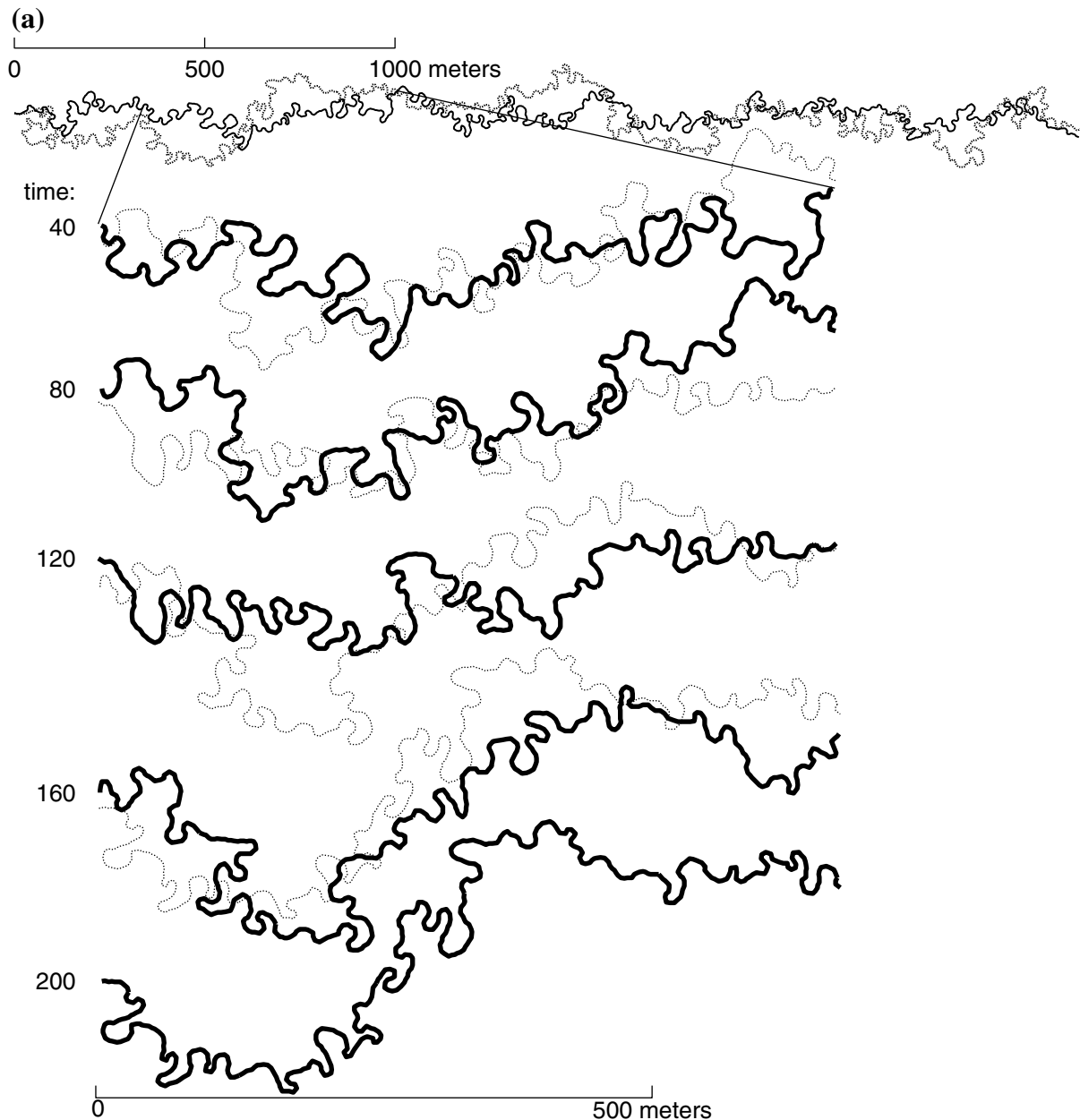


Figure 17. Simulations showing sensitivity to the parameter,  $\lambda$ . Model channel evolution with (a)  $\lambda = 4.0\text{m}$ ; and (b)  $\lambda = 15\text{m}$ . For (a) and (b), at top, channels at 40 (solid) and 200 (dotted) time units are superimposed. Below, a part is enlarged and shown at 40, 80, 120, 160, and 200 time units, from top to bottom. For all but the last time, the next time is superimposed as a dotted line.

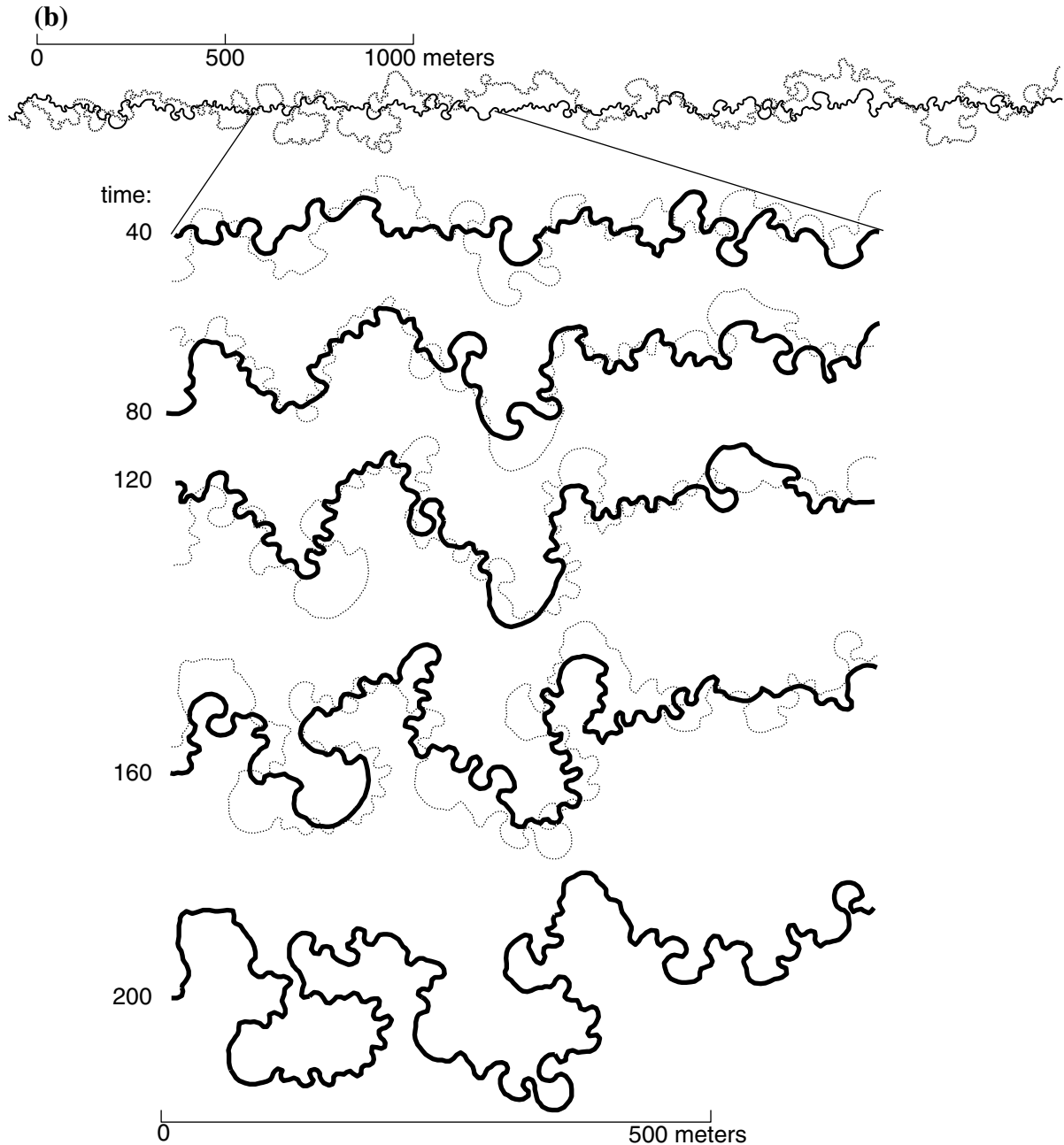


Figure 17. (Continued)

tion could potentially affect the downstream lag,  $L$ , we found that finer discretization led to smaller bends but no change in compound bend formation. The discretization's affect on the 'texture' of the simulated form is not unusual to this model. In our own experience with landscape evolution models the horizontal discretization of topography affects simulated landscape texture such that finer discretizations can lead to higher drainage densities (Lancaster, 1998).

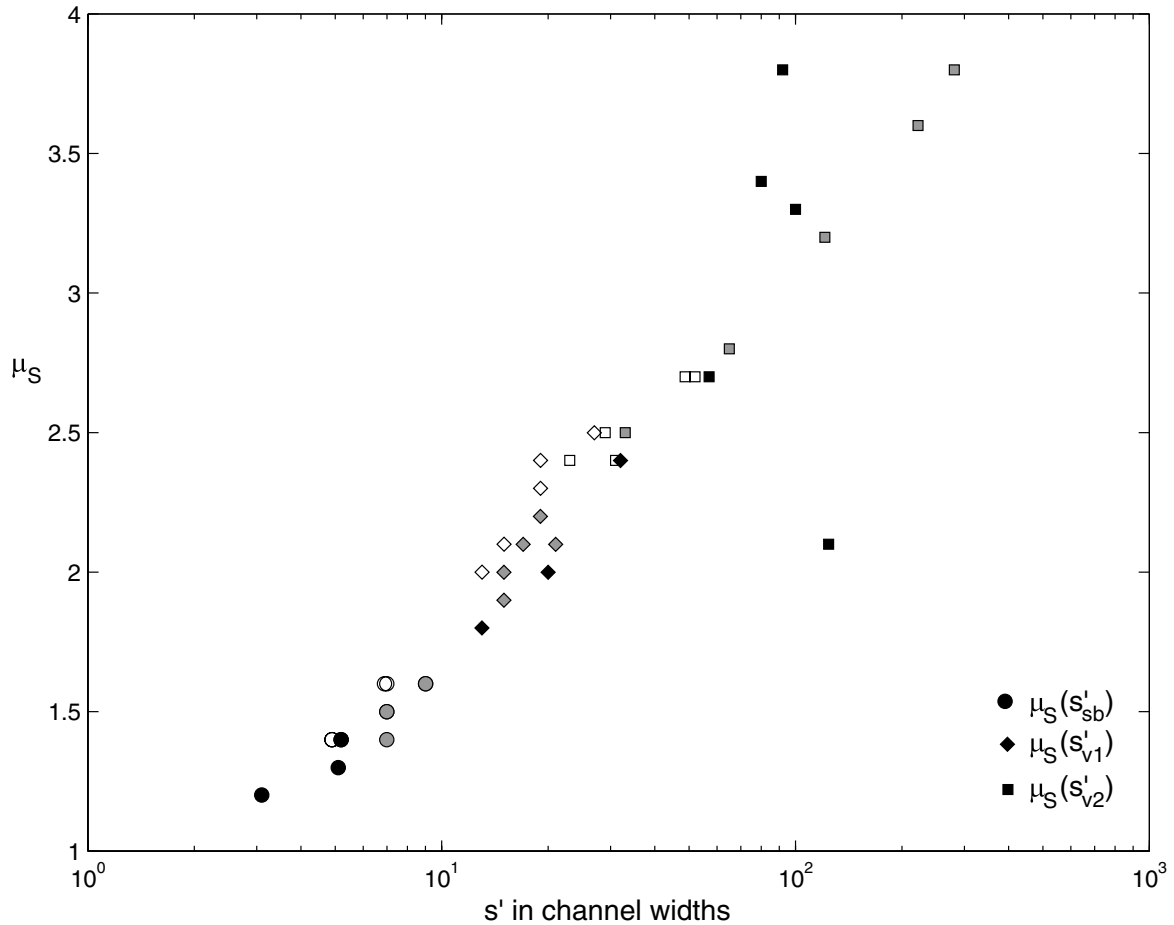


Figure 18.  $\mu_S(s'_{sb})$ ,  $\mu_S(s'_{v1})$ , and  $\mu_S(s'_{v2})$  for channels simulated with  $\lambda = 4.0\text{m}$  (open symbols),  $\lambda = 8.0\text{m}$  (default, gray symbols), and  $\lambda = 15\text{m}$  (black symbols)

Table VI. Summary of compound bend formation's sensitivity to parameters through downstream lag,  $L$

Parameter	Relationship to $L$	Effect of increase on compound bend formation
$S_v$	$L \sim S_v^{-0.35}$	Slight increase
$d_{50}$	Sub-linear	Slight decrease
$\Delta s$	Possibly, $L \sim \Delta s$	None

### CONCLUSIONS

The key results are:

1. Our planform analysis reveals that in many natural meandering streams multi-bend loops, which result from formation and division of compound bends, are important contributors to planform sinuosity.

2. Previous, physics-based models, e.g., the JP model, do not accurately reproduce this contribution.
3. Our new model, with its simplified process representation, is sufficient to produce realistic meander evolution, during which compound bend and multi-bend loop formation emerge as primary mechanisms of planform evolution.
4. The model predicts that compound bend and multi-bend loop formation are sensitive to the interaction between two important lengths, the downstream lag between the bend entrance and the zone of maximum bank shear stress,  $L$ , and the distance over which that shear stress is dissipated,  $\lambda$ . Specifically, larger values of  $\lambda$ , which correspond to smoother banks, lead to greater importance of multi-bend loop formation to planform sinuosity.

The implications for natural streams are that (i) multi-bend loops may result from primary process mechanisms rather than secondary phenomena, such as bank heterogeneity or alternate bars, and (ii) the prevalence of multi-bend loop formation may be sensitive to bank roughness. Our analysis measures the prevalence of multi-bend loop formation, and bank roughness can be measured in the field or, perhaps, inferred from characteristics, such as bank vegetation, detectable with remote sensing. These implications, therefore, represent a testable hypothesis motivating future work.

#### ACKNOWLEDGEMENTS

This research was supported by the U.S. Army Construction Engineering Research Laboratories (DACA 88-95-R-0020) while the first author was at the Massachusetts Institute of Technology. The views, opinions, and/or findings contained in this paper are those of the authors and should not be construed as an official Department of the Army position, policy, or decision, unless so designated by other documentation. This research has also been supported by the CLAMS Project, Pacific Northwest Research Station of the USDA Forest Service, since the first author moved to Oregon State University. We are grateful to Gordon Grant, Shannon Hayes, Gregory Tucker, and Kelin Whipple for discussion and thoughtful comments, Jim Pizzuto for a helpful review of an earlier version, and Rob Ferguson and an anonymous reviewer for helpful reviews.

#### APPENDIX: THE JP MODEL

##### *The JP Model*

The JP model assumes bank shear stress and channel migration are proportional to the near-bank flow velocity perturbation:

$$u_{b1} = \chi_{20} Ub C(s) + \frac{C_f Ub^2}{H} \left[ \chi_{20} \left( \frac{U^2}{gH} + 2 \right) - 1 \right] e^{\frac{-2C_f s}{H}} \int_0^s C(s') e^{\frac{2C_f s'}{H}} ds' \\ \dots + \frac{C_f Ub}{H} (K + A_s) e^{\frac{-2C_f s}{H}} \int_0^s C(s') e^{\frac{2C_f s'}{H}} ds' \quad (\text{A1})$$

$$A_s = \frac{181}{\chi_1} \left( \frac{2H}{b} \right)^2 \left( 2\chi^2 + \frac{4\chi}{5} + \frac{1}{15} \right) \quad (\text{A2})$$

$$\chi_{20} = \frac{1}{\chi_1^3} \left( \chi^3 + \chi^2 + \frac{2\chi}{5} + \frac{2}{35} \right), \chi_1 = \frac{0.077}{\sqrt{C_f}}, \chi = \frac{0.077}{\sqrt{C_f}} - \frac{1}{3} \quad (\text{A3})$$

where we have made one simplification from Johannesson and Parker (1989c): we have substituted local curvature,  $C$ , for the effective curvature integral in the argument of the second integral in Equation (A1).

This substitution makes the JP model more directly comparable to ours, and A.D. Howard (personal communication, 1996) reports that the use of effective curvature rather than local curvature has an insignificant effect on model behaviour.

## REFERENCES

- Andrle R. 1994. The angle measure technique: A new method for characterizing the complexity of geomorphic lines. *Mathematical Geology* **26**: 83-97.
- Andrle R. 1996. Measuring channel planform of meandering rivers. *Physical Geography* **17**(3): 270-281.
- Beck S. 1984. Mathematical modeling of meander interaction. In *River Meandering*, Proceedings of the Conference, Rivers '83, Elliott CM (ed). ASCE: New York; 932-941.
- Blondeaux P, Seminara G. 1985. A unified bar-bend theory of river meanders. *Journal of Fluid Mechanics* **157**: 449-470.
- Brice J. 1974. Meandering pattern of the White River in Indiana--an analysis. In *Fluvial Geomorphology*, Morisawa M (ed). State University of New York: Binghamton; 178-200.
- Dietrich WE, Smith JD. 1983. Influence of the point bar on flow through curved channels. *Water Resources Research* **19**(5): 1173-1192.
- Dietrich WE, Smith JD. 1984. Bed load transport in a river meander. *Water Resources Research* **20**(10): 1355-1380.
- Dietrich WE, Whiting P. 1989. Boundary shear stress and sediment transport in river meanders of sand and gravel. In *River Meandering*, Ikeda S, Parker G (eds). American Geophysical Union: Washington; 1-50.
- Engelund F, Hansen F. 1967. A monograph on sediment transport in alluvial streams. In *Teknisk Verlag*. Technical University of Denmark: Copenhagen; 63.
- Ferguson RI. 1984. Kinematic model of meander migration. In *River Meandering*, Proceedings of the Conference, Rivers '83, Elliott CM (ed). ASCE: New York; 942-951.
- Furbish DJ. 1988. River-bend curvature and migration: How are they related? *Geology* **16**: 752-755.
- Furbish DJ. 1991. Spatial autoregressive structure in meander evolution. *GSA Bulletin* **103**(12): 1576-1589.
- Hasegawa K. 1989. Studies on qualitative and quantitative prediction of meander channel shift. In *River Meandering*, Ikeda S, Parker G (eds). American Geophysical Union: Washington; 215-235.
- Hooke JM, Harvey AM. 1983. Meander changes in relation to bend morphology and secondary flows. *Modern and Ancient Fluvial Systems*, Collinson JD, Lewin J (eds). Special Publication of the International Association of Sedimentologists **6**: 121-132.
- Howard AD. 1992. Modelling channel migration and floodplain development in meandering streams. In *Lowland Floodplain Rivers*, Carling PA, Petts GE (eds). John Wiley & Sons: Chichester; 1-42.
- Howard AD. 1994. A detachment-limited model of drainage basin evolution. *Water Resources Research* **30**(7): 2261-2285.
- Howard AD, Hemberger AT. 1991. Multivariate characterization of meandering. *Geomorphology* **4**: 161-186.
- Howard AD, Knutson TR. 1984. Sufficient conditions for river meandering: A simulation approach. *Water Resources Research* **20**(11): 1659-1667.
- Ikeda S. 1989. Sediment transport and sorting at bends. In *River Meandering*, Ikeda S, Parker G (eds). American Geophysical Union: Washington; 103-126.
- Ikeda S, Parker G, Sawai K. 1981. Bend theory of river meanders. Part 1. Linear development. *Journal of Fluid Mechanics* **112**: 363-377.
- Ikeda S, Yamasaka M, Chiyoda M. 1987. Bed topography and sorting in bends. *Journal of Hydraulic Engineering* **113**(2): 190-206.
- Imran J, Parker G, Pirmez C. 1999. A nonlinear model of flow in meandering submarine and subaerial channels. *Journal of Fluid Mechanics* **400**: 295-331.
- Johannesson H, Parker G. 1985. Computer simulated migration of meandering rivers in Minnesota. *Project Report No. 242*. St. Anthony Falls Hydraulic Laboratory: Minneapolis; 82.
- Johannesson H, Parker G. 1989a. Linear theory of river meanders. In *River Meandering*, Ikeda S, Parker G (eds). American Geophysical Union: Washington; 181-214.
- Johannesson H, Parker G. 1989b. Secondary flow in mildly sinuous channel. *Journal of Hydraulic Engineering* **115**(3): 289-308.
- Johannesson H, Parker G. 1989c. Velocity redistribution in meandering rivers. *Journal of Hydraulic Engineering* **115**(8): 1019-1039.
- Lancaster ST. 1998. *A Nonlinear River Meandering Model and its Incorporation in a Landscape Evolution Model*. Ph.D. Thesis, Dept. of Civil and Environmental Engineering, Massachusetts Institute of Technology: Cambridge; 277.
- Murray AB, Paola C. 1994. A cellular model of braided rivers. *Nature* **371**(6492): 54-57.
- Murray AB, Paola C. 1997. Properties of a cellular braided-stream model. *Earth Surface Processes and Landforms* **22**: 1001-1025.
- Nanson GC, Hickin EJ. 1983. Channel migration and incision on the Beatton River. *Journal of Hydraulic Engineering* **109**: 327-337.
- Nelson JM, Smith JD. 1989a. Flow in meandering channels with natural topography. In *River Meandering*, Ikeda S, Parker G (eds). American Geophysical Union: Washington; 69-102.
- Nelson JM, Smith JD. 1989b. Evolution and stability of erodible channel beds. In *River Meandering*, Ikeda S, Parker G (eds). American Geophysical Union: Washington; 321-378.
- Odgaard AJ. 1982. Bed characteristics in alluvial channel bends. *Journal of the Hydraulics Division* **108**(HY11): 1268-1281.
- Odgaard AJ. 1986. Meander flow model. I: Development. *Journal of Hydraulic Engineering* **112**(12): 1117-1136.
- Paola C, Hellert PL, Angevine CL. 1992. The large-scale dynamics of grain-size variation in alluvial basins, 1: Theory. *Basin Research* **4**: 73-90.
- Parker G, Sawai K, Ikeda S. 1982. Bend theory of river meanders. Part 2. Nonlinear deformation of finite-amplitude bends. *Journal of Fluid Mechanics* **115**: 303-314.

- Pizzuto JE, Meckelnburg TS. 1989. Evaluation of a linear bank erosion equation. *Water Resources Research* **25**: 1005-1013.
- Seminara G, Tubino M. 1989. Alternate bars and meandering: Free, forced and mixed interactions. In *River Meandering*, Ikeda S, Parker G (eds). American Geophysical Union: Washington; 267-320.
- Seminara G, Tubino M. 1992. Weakly nonlinear theory of regular meanders. *Journal of Fluid Mechanics* **244**: 257-288.
- Smith JD, McLean SR. 1984. A model for flow in meandering streams. *Water Resources Research* **20**(9): 1301-1315.
- Sun T, Meakin P, Jøssang T, Schwarz K. 1996. A simulation model for meandering rivers. *Water Resources Research* **32**(9): 2937-2954.
- Thompson A. 1986. Secondary flows and the pool-riffle unit, a case study of the processes of meander development. *Earth Surface Processes and Landforms* **11**(6): 631-641.
- Thorne CR, Osman AM. 1988. Riverbank stability analysis, II, applications. *Journal of Hydraulic Engineering* **114**(2): 151-172.
- Thorne SD, Furbish DJ. 1995. Influences of coarse bank roughness on flow within a sharply curved river bend. In *Predicting Process from Form*, Whiting PJ, Furbish DJ (eds). *Geomorphology* **12**(3): 241-257.
- Tucker GE, Slingerland RL. 1994. Erosional dynamics, flexural isostasy, and long-lived escarpments: a numerical modeling study. *Journal of Geophysical Research* **99**: 12,229-12,243.
- Willgoose G, Bras RL, Rodriguez-Iturbe I. 1991. A physically based coupled network growth and hillslope evolution model, 1, theory. *Water Resources Research* **27**: 1671-1684.
- Zhou J, Chang H-H, Stow D. 1993. A model for phase lag of secondary flow in river meanders. *Journal of Hydrology* **146**(1-4): 73-88.